Catalysis Letters (2024) 154:191–205
https://doi.org/10.1007/s10562-023-04283-5

# Preparation of Pt/$MgAl_2O_4$ Decalin Dehydrogenation Catalyst for Chemical Hydrogen Storage Application

Fengli Wang[1,2] · Mingsheng Luo[1,2] · Qinglong Liu[1,2] · Changke Shao[1,2] · Zhi Yang[1,3] · Xinyue Liu[1,2] · Jiakun Guo[1]

Received: 16 October 2022 / Accepted: 17 January 2023 / Published online: 10 February 2023


## Abstract

Chemical hydrogen storage is an important area for hydrogen fuel cell applications while catalyst is the key to develop effective hydrogen production process for fuel cell applications. Platinum is a superior catalyst for decalin dehydrogenation, and support modification can improve the catalysis. Effects of different supports, preparation methods and Mg/Al molar ratio on the material properties and the catalytic performance of the Pt catalysts were thus systematically investigated. The results showed that the $MgAl_2O_4$ support was more suitable for improving Pt dispersion and forming smaller Pt nanoparticles than the others. The Pt/$MgAl_2O_4$ with Mg/Al molar ratio of 0.5 prepared by alcohol-heating method demonstrated superior performance, which is closely related to the Pt nanoparticle size and reaction state. Initial ratio of decalin to catalyst also played an important role in the activity and was achieved the optimal ratio in the liquid-film state.

## Graphical Abstract

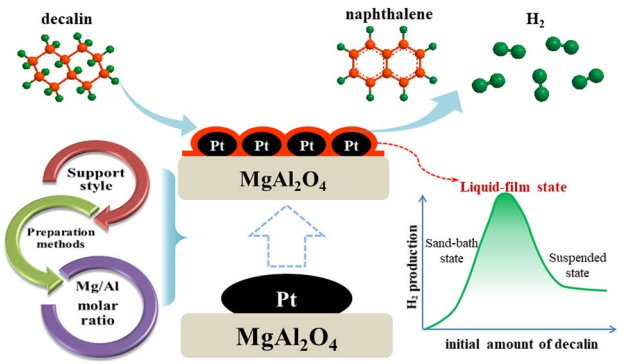


**Keywords** Chemical hydrogen storage · Pt · $MgAl_2O_4$ catalyst · Decalin dehydrogenation · Tetralin · Naphthalene hydrogenation

✉ Mingsheng Luo
luoms9297@163.com

✉ Qinglong Liu
lql@bipt.edu.cn

[1] College of New Materials and Chemical Engineering, Beijing Institute of Petrochemical Technology, 19 Qing-Yuan North Road, Beijing 102600, China

[2] Beijing Key Laboratory of Fuels Cleaning and Advanced Catalytic Emission Reduction Technology, Beijing Institute of Petrochemical Technology, 19 Qing-Yuan North Road, Beijing 102600, China

[3] Faculty of Environment and Life Science, Beijing University of Technology, 100 Ping-Le-Yuan, Beijing 100124, China

## 1 Introduction

The increasing fossil fuel consumption and the climate change due to the vast $CO_2$ emission force people to develop green and renewable energy [1]. As an efficient and clean energy, hydrogen shows a good application prospect in solving energy crisis and alleviating air pollution. Hydrogen energy utilization includes hydrogen production, storage, transportation and application, among which hydrogen energy storage is one of the key and difficult tasks [2, 3]. Organic liquid hydrogen storage technology using

methylcyclohexane, cyclohexane, decahydronaphthalene (decalin) or tetrahydronaphthalene (tetralin) is based on reversible hydrogenation and dehydrogenation reaction cycle, which has been of great interest due to the high hydrogen storage density, convenient transportation and carbon-free emission in the hydrogen storage process and meeting the requirements of green chemistry [4–11]. Our earlier research shows that tetralin was an effective hydrogen carrier in coal liquefaction related reactions, in which hydrogen can be transferred effectively by tetralin/decalin solvent to the coal in hydrogenation reaction [12]. This leads us to the idea to utilize the same hydrogen carrier, i.e., decalin or/and tetralin here as a chemical storage carrier for hydrogen energy applications. As a commercially available liquid organic hydrogen carriers, decalin can provide a high hydrogen storage density (7.3 wt %), while decalin is an environmentally friendly hydrogen carrier with no carbon dioxide emission in the dehydrogenation process [13–16].

In the liquid organic hydrogen storage technology, hydrogenation technology is relatively mature, but dehydrogenation technology still faces some challenges. Dehydrogenation process is always an endothermic reaction with increasing volume of products. High temperature and low pressure are conducive to the dehydrogenation reaction, but side reactions such as hydrogenolysis and coking are easy to occur at high temperature, which reduces the activity, selectivity and stability of the dehydrogenation catalyst and thus hinders the reversible cycle of hydrogenation and dehydrogenation. Therefore, the development of low-temperature and high-efficiency dehydrogenation catalyst has become the key area in liquid organic hydrogen storage technology.

Supported catalysts are widely used in commercial chemical industrial applications. The support material not only provides a carrier for the loading of active metals, but also improves the physicochemical properties and the catalytic performance of the catalyst. Martynenko et al. studied the catalytic activity of Pt-based catalysts supported on the common support including $Al_2O_3$, $SiO_2$ and mesoporous silica SBA-15 and MCM-48 for the catalytic dehydrogenation of decalin [17]. They found that the mesoporous silica SBA-15 and MCM-48 supported Pt catalysts showed higher catalytic activity compared with the $Al_2O_3$ or $SiO_2$ supported Pt catalysts. SBA-15 and MCM-48 supports had high specific surface area and sufficient pore volume, and showed a good steric effect. Carbon is also a common support material in decalin dehydrogenation catalysts. Sebastian et al. used industrial activated carbon to prepare Pt/C catalyst for decalin dehydrogenation, and found that the conversion was close to thermodynamic equilibrium [18]. Among various carbon materials, carbon nanofibers (CNFs) offer much more exposed surface area than the others, which can facilitate the inner pore diffusion process. For example, Li et al synthesized carbon nanofibers (CNFs) with different microstructures as the support of Pt-based decalin dehydrogenation catalyst [19]. Their results showed that the Pt/CNFs catalyst with platelet microstructure was proved to be highly efficient in catalytic dehydrogenation of decalin. Tuo et al. synthesized two types of structured CNFs as support materials to prepare Pt catalysts for dehydrogenation of decalin. It was found that the dehydrogenation effect was significantly better than that of AC. [20]. They further investigated the influence of Pt particle size on the dehydrogenation process of decalin on CNFs and CNTs. Their results showed that for Pt particles smaller than 2 nm, the consequent catalytic activity between Pt/CNFs and Pt/CNTs is dominated by the carbon support effect and the particle size effect became important when Pt particles were larger than 2 nm [21].

Carbon materials have unique advantages in structural regulation and surface functionalization. However, the influencing factors such as preparation process, cost and stability of the carbon nanomaterials as the support of catalysts should be considered in application of the support material. $MgAl_2O_4$ is widely used as catalyst support because of excellent properties, i.e., high thermal stability, unique surface properties of both acidic and basic active centers, low thermal expansion coefficient and high mechanical strength [22–27]. In particular, the preparation methods had a marked effect on specific surface area, pore structure and metallic particle dispersion and mechanical strength of $MgAl_2O_4$ support [28, 29]. Wang et al. compared the effects of different preparation methods of Pt/$MgAl_2O_4$ on the partial oxidation of methane to syngas and demonstrated that the catalyst synthesized via hydrolysis solvothermal method exhibited more excellent catalytic performance than that by co-precipitation method [30]. Tuo et al. found that the Pt/$MgAl_2O_4$ catalyst showed much better activity than Pt/CNF catalyst for decalin dehydrogenation [31]. The enhanced activity arose from the partially positive-charged Pt as a result of the strong interactions between Pt and the surface oxygen atoms of $MgAl_2O_4$. Thus, an outstanding decalin dehydrogenation activity nearly twice of corresponding Pt/CNF catalyst was achieved. To our knowledge, the influence of the regulation of $MgAl_2O_4$ synthesis conditions on the catalyst in the dehydrogenation of decalin has not been reported yet so far.

Hodoshima et al. found that the ratio of liquid decalin to solid catalyst had a significant effect on the conversion of decalin to $H_2$ and naphthalene [32]. The highest catalytic activity of decalin dehydrogenation was accomplished at 3.3 mL/g ratio of decalin to catalyst. In this case, the carbon supported catalyst was wet rather than suspended in the whole reaction process. The surface of catalyst was covered with a layer of liquid matrix film, which was called "liquid-film state". Kariya et al also found that the dehydrogenation rate of cycloalkanes was significantly dependent on the initial feeding amounts. The hydrogen evolution rate in the

liquid-film state seemed to be the largest, and each reactant had its own optimal initial feed amount [33].

In this work, four common support materials including alumina ($Al_2O_3$), mesoporous silica (MCM-41), activated carbon (AC) and magnesium aluminate ($MgAl_2O_4$) were selected to prepare the Pt-based catalysts, and the results showed that the $MgAl_2O_4$ was the better support than the others. Subsequently, $MgAl_2O_4$ was separately prepared by alcohol-heating, sol–gel, co-precipitation and solid reaction methods. The as-synthesized $MgAl_2O_4$ materials were used as support to prepare Pt/$MgAl_2O_4$ catalysts. In addition, the physicochemical properties of all the catalysts were characterized by X-ray diffraction, Nitrogen adsorption/desorption, scanning electron microscopy, transmission electron microscopy and $NH_3$-temperature programmed desorption techniques. The influence of $MgAl_2O_4$ support prepared by different methods on the catalytic performance for the dehydrogenation of decalin was discussed. Effect of Mg/Al molar ratio was also studied before the optimized decalin/catalyst ratio of the reaction system was determined in this work.

## 2 Experimental

### 2.1 Catalyst Preparation

#### 2.1.1 Preparation of $MgAl_2O_4$

$MgAl_2O_4$ support was prepared by four different methods as follows.

**2.1.1.1 Alcohol-Heating Method** 0.01 mol magnesium nitrate hexahydrate and 0.02 mol aluminum isopropoxide were mixed in 30 mL of ethanol and stirred at 40 °C for 1 h. Then, the solution was placed in a Teflon autoclave at 150 °C for 12 h. A clear yellow suspension was obtained after alcohol heating. Then, the ethanol was removed by rotary evaporator and the resulting gel was dried at 90 °C overnight. Finally, the dried powders were calcined in air at 800 °C for 12 h with a heating rate of 5 °C $min^{-1}$. The sample prepared by the alcohol-heating method was named as $MgAl_2O_4$-AH.

**2.1.1.2 Sol–Gel Method** At first, 1.5 g of P123, i.e., polyethene oxide (PEO)-polypropene oxide (PPO)-PEO, was added into 30 mL of ethanol and stirred vigorously until it is completely dissolved. Then, 1.28 g magnesium nitrate hexahydrate was added to the above solution. After the solution is clarified, 2.04 g of aluminum isopropoxide and 2.4 mL of concentrated nitric acid were added into the above mixed solution. Subsequently, the mixed solution was transferred into the drying oven at 70 °C for 48 h to get a dried gel. Finally, the dried gel precursor was calcined at 700 °C for 8 h with a heating rate of 5 °C $min^{-1}$. The sample prepared by the sol–gel method was named as $MgAl_2O_4$-SG.

**2.1.1.3 Co-precipitation Method** 0.01 mol magnesium nitrate hexahydrate and 0.02 mol aluminum nitrate were solved in 100 mL deionized water. Then, ammonia aqueous solution was added drop by drop into the above solution to produce white precipitation at pH9.5 and stirred for another 12 h. Subsequently, the precipitation was centrifuged and dried at 90 °C for 12 h. Finally, the powders were calcined in air at 800 °C for 12 h with a ramp of 5 °C $min^{-1}$. The sample prepared by the co-precipitation method was denoted as $MgAl_2O_4$-CP.

**2.1.1.4 Solid Reaction Method** 0.02 mol magnesium nitrate hexahydrate, 0.02 mol aluminum nitrate and 0.06 mol citric acid were ball-milled for 1 h using a horizontal ball mill. The pulverized mixture was placed in an oven at 100 °C for 2 h to promote the proper fusion of the $Al^{3+}$ and $Mg^{2+}$ precursors. Finally, the mixture was calcined at 700 °C for 5 h with a heating rate of 5 °C $min^{-1}$. The sample prepared by the solid reaction method was named as $MgAl_2O_4$-SR.

#### 2.1.2 Preparation of Pt/$MgAl_2O_4$ Catalyst

Pt/$MgAl_2O_4$ catalysts were prepared by the excessive impregnation method. The supports were completely immersed into an appropriate concentration aqueous solution of chloroplatinic acid aqueous solution to achieve Pt loading of 1 wt%. During the impregnation, the mixture was stirred rigorously for 2 h. Then, the solution was heated at 80 °C and stirred continuously until the liquid was totally eliminated. Subsequently, the impregnated samples was dried overnight at 80 °C and then reduced for 3 h at 300 °C with a flowing $H_2$ gas. The final Pt loading of the catalysts was in the range of 0.8–0.9 wt% per actual ICP-OES result.

### 2.2 Catalyst Characterization

X-ray diffraction (XRD) of catalysts was performed on the SmartLab 9KW diffractometer equipped with a Cu Kα source (λ = 1.5418 Å) at 40 kV and 30 mA. The samples were scanned from 2θ = 5 to 80° with a scanning rate of 4°/min. The morphological characteristics of catalysts were observed using scanning electron microscopy (GeminiSEM 300) and transmission electron microscopy (JEOL JEM-F200). Nitrogen adsorption/desorption isotherms were measured with the BELSORP-max apparatus at − 196 °C. Before analysis, the samples were degassed at 400 °C for 4 h under vacuum condition. XPS spectra were recorded by Thermo Scientific analyzer equipped with Al Kα radiation. Inductively coupled plasma optical emission spectrometry (ICP-OES) was used to determine the Pt loading

on ICPE-9800. $NH_3$-temperature programmed desorption ($NH_3$-TPD) tests were performed to determine the surface acidity of the catalyst sample. 0.1 g sample was pretreated in flowing He (30 mL/min) at 300 °C for 1 h, followed by $NH_3$ saturated adsorption at 50 °C, and then flushed with flowing He at the same temperature for 1 h. $NH_3$-TPD experiments were performed using a temperature ramp from 30 to 600 °C at a heating rate of 10 °C $min^{-1}$. CO chemisorption was measured by the Micromeritics AutoChem II 2920 equipped with a thermal conductivity detector (TCD).

### 2.3 Catalytic Activity Evaluation

The catalytic activities of catalysts for decalin dehydrogenation were evaluated using a batch-wise reactor. The batch-wise reactor consisted of a 50 mL three-necked flask, fitted with a condenser in the central opening. Typically, 0.3 g catalyst was placed at the bottom of the flask to form a thin layer, and 1 mL decalin was added dropwise into the flask to ensure that the catalyst is properly wetted. Then, the flask was purged with $N_2$ for 20 min to remove $O_2$. When the electric heating jacket was heated to the preset reaction temperature, and the flask was placed in the heating jacket to start the reaction. The volume of $H_2$ released during the reaction was monitored by the volume of water replaced in the U-tube. In addition, blank experiments were carried out on the various $MgAl_2O_4$ supports to eliminate the catalytic effect of supports on decalin dehydrogenation.

## 3 Results and Discussion

### 3.1 Comparison of Support of Pt-based Catalysts

Four common supports including $Al_2O_3$, mesoporous silica (MCM-41), activated carbon (AC) and $MgAl_2O_4$-AH prepared by the alcohol-heating method were selected to prepare the supported Pt-based catalysts, and the properties of catalysts were characterized by a variety of techniques. Then the corresponding catalytic activities of catalysts for decalin dehydrogenation were evaluated in a batch reactor.

The XRD patterns of different supports (Fig. S1) and Pt-based catalysts are basically consistent with the characteristic peaks of the corresponding support (Fig. 1). Pt/MCM-41 and Pt/AC show a wide peak at about 21.5°, indicating that these supports were typical amorphous phases [34]. The sharp XRD peaks at 19.0°, 31.3°, 36.8°, 44.7°, 55.8°, 59.4°, 65.2° and 77.2° are ascribed to the diffraction of spinel $MgAl_2O_4$. The peaks of Pt/$Al_2O_3$ at 37.6°, 45.8° and 66.8° are assigned to γ-$Al_2O_3$ (JCPDS No.10-0425) with good crystallinity. For Pt/MCM-41 and Pt/AC, the three sharp characteristic peaks at 39.8°, 46.2°, and 67.5° ascribed to Pt (111), (200), (220) facet(JCPDS No. 04-0802). The results showed that AC was easy to cause Pt species to form large nanoparticles. In contrast, no significant peaks assigned to the Pt nanoparticles are observed for the Pt/$MgAl_2O_4$ and Pt/$Al_2O_3$ catalysts. It may be due that the Pt species interact strongly with $MgAl_2O_4$ and $Al_2O_3$ and exist in a highly dispersed state with single atom or small nanoparticles.

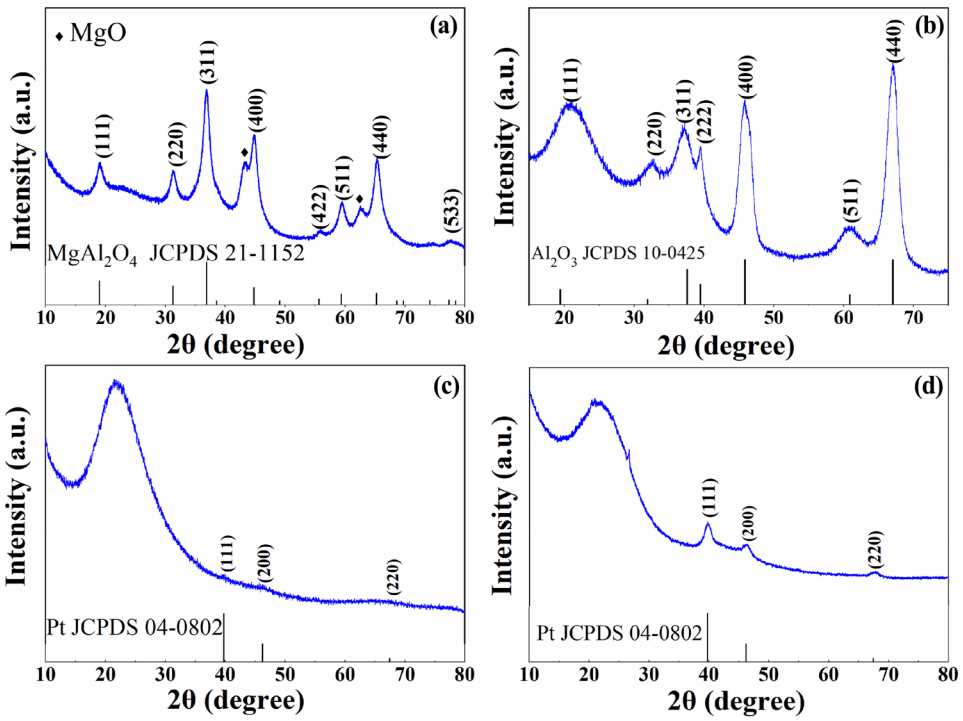


**Fig. 1** XRD patterns of the **a** Pt/$MgAl_2O_4$-AH, **b** Pt/$Al_2O_3$, **c** Pt/MCM-41 and **d** Pt/AC

The nitrogen adsorption/desorption isotherm and pore size distribution of the supports and catalysts are shown in Figs. S2 and S3. It can be concluded that Pt/$MgAl_2O_4$-AH, Pt/$Al_2O_3$ and Pt/MCM-41 exhibited the classical shape of type IV isotherm according to the IUPAC classification, which were typical mesoporous solids; but the isotherm shape of Pt/AC was type I, which represented microporous adsorption. It could be seen from Table 1 that the specific surface area followed the sequence of Pt/AC > Pt/MCM-41 > Pt/$MgAl_2O_4$-AH > Pt/$Al_2O_3$. The Pt/AC sample showed the largest specific surface area of 1317 $m^2$/g, but appeared many Pt nanoparticles as proved by the XRD results. The Pt species should be mainly located on the outer surface during the impregnation process and then easy to form the large nanoparticles at high reduction temperature. Due to the mesopore-confined effect of MCM-41, the average size of Pt particles was about 4.29 nm similar to the mean pore size of MCM-41 support. Although the Pt/$MgAl_2O_4$-AH and Pt/$Al_2O_3$ samples exhibited small specific surface area and large mean pore size, the corresponding average particle size of Pt species were obviously smaller than Pt/MCM-41 and Pt/AC. It might be that the strong interaction between Pt species and $MgAl_2O_4$-AH inhibited the Pt nanoparticles growth.

**Table 1** Textural properties and particle size of Pt-based catalysts with different supports

| Catalysts | $S_{BET}$[a] ($m^2$ $g^{-1}$) | $V_p$[b] ($cm^3$ $g^{-1}$) | $D_m$[c] nm | Average particle size of Pt (nm)[d] |
|---|---|---|---|---|
| Pt/$MgAl_2O_4$ | 307 | 0.92 | 11.3 | 1.24 |
| Pt/$Al_2O_3$ | 156 | 0.91 | 23.2 | 2.23 |
| Pt/MCM-41 | 826 | 0.81 | 4.0 | 4.29 |
| Pt/AC | 1317 | 0.99 | 3.0 | 9.02 |

[a]$S_{BET}$ is the specific surface area calculated by BET method

[b]$V_p$ is the total pore volume

[c]$D_m$ is the mean pore diameter

[d]Average Pt particle size obtained by fitting TEM data

The average particle size and the dispersion of Pt species were characterized by TEM. The larger metallic platinum particles can be observed on the Pt/MCM-41 and Pt/AC samples than the Pt/$MgAl_2O_4$-AH and Pt/$Al_2O_3$ samples as shown in Fig. 2, indicating that the Pt species were easy to agglomerate and form larger Pt nanoparticles on the MCM-41 and AC support. It is consistent with the XRD results. Pt/$MgAl_2O_4$-AH catalyst shows a quite narrow distribution of Pt nanoparticle size in the range of 0.5–2.5 nm, but Pt/

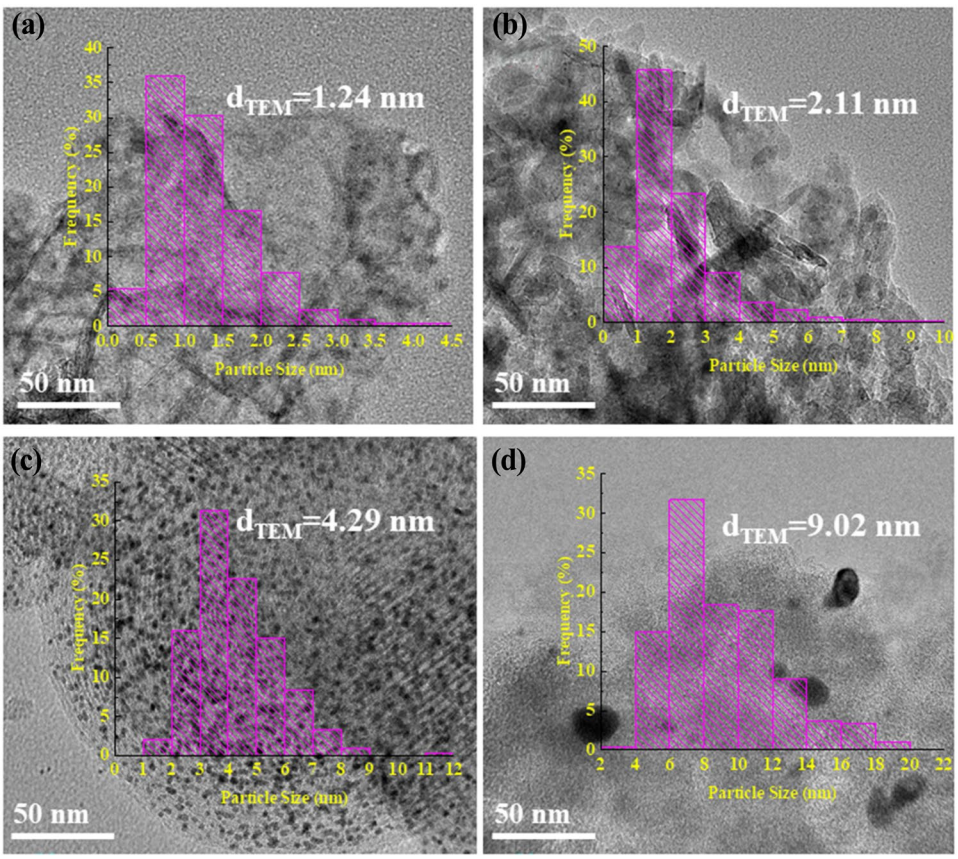


**Fig. 2** TEM images and the corresponding particle size distributions of Pt-based catalysts with different supports: **a** Pt/$MgAl_2O_4$-AH; **b** Pt/$Al_2O_3$; **c** Pt/MCM-41; **d** Pt/AC

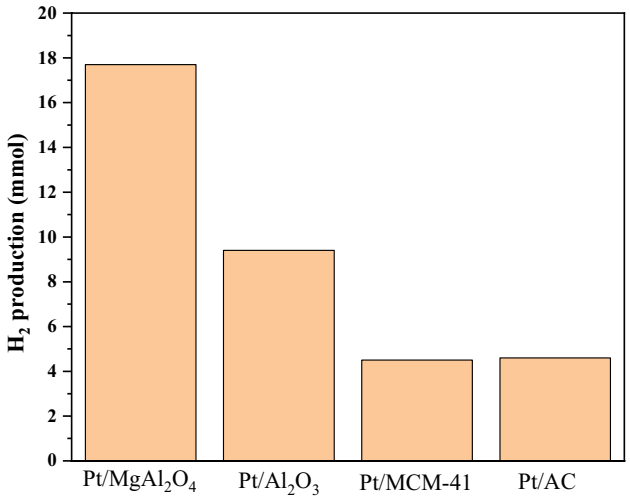


**Fig. 3** The hydrogen production of Pt-based catalysts with different supports. Reaction condition: 2.5 h, 260℃, 0.3 g of catalyst and 1 mL of decalin

$Al_2O_3$, Pt/MCM-41 and Pt/AC exhibit the broad distribution in the range of 0.5–6 nm, 2–8 nm and 4–18 nm.

Figure 3 shows the comparison diagram of hydrogen production in 2.5 h under the conditions of 260 °C, 0.3 g of catalyst and 1 ml of decalin. It is found that the catalytic activities are in the order of Pt/$MgAl_2O_4$-AH > Pt/$Al_2O_3$ > Pt/MCM-41 > Pt/AC. Obviously, Pt/$MgAl_2O_4$-AH catalyst yields the best catalytic performance, and the hydrogen production in 2.5 h was almost twice that of Pt/$Al_2O_3$ and more than 4 times that of Pt/MCM-41 or Pt/AC.

According to the literature reported by Sebastian et al. [18], it was found that Pt particle size was one of the critical factors in determining the catalytic activity of decalin dehydrogenation. Generally, the smaller Pt particle size is, the higher activity is. For the Pt-based catalysts prepared by different supports, the Pt particle sizes follow the order of Pt/$MgAl_2O_4$-AH < Pt/$Al_2O_3$ < Pt/MCM-41 < Pt/AC, and the catalytic activity also follows this order. These results demonstrate that the size of Pt nanoparticle plays a dominant role in catalytic performance for the decalin dehydrogenation. Generally, a large specific surface area of support can provide more accessible sites to the reactant molecules, but the interaction between Pt and support should be the key factor for the Pt nanoparticle size. Among all selected catalysts, Pt/MCM-41 and Pt/AC displayed relatively highest surface area and pore volume, but generated largest Pt nanoparticle because of the serious agglomeration of Pt species. The obvious difference in catalytic activity was mainly due to the Pt nanoparticle size resulting from the different supports.

Therefore, the type of support exerts a determining effect on the activity of the catalyst. The Pt-based catalyst prepared with $MgAl_2O_4$ prepared by the alcohol-heating method produced the highest catalytic activity. This provides a possible basis for the preparation of superior Pt-based catalysts for decalin dehydrogenation. In order to modify the Pt/$MgAl_2O_4$ catalyst, the effect of different preparation methods of $MgAl_2O_4$ support on the Pt/$MgAl_2O_4$ catalyst was further investigated.

## 3.2 Effect of Preparation Method of $MgAl_2O_4$

Figure 4a, b showed the XRD patterns of $MgAl_2O_4$ supports and Pt/$MgAl_2O_4$ catalysts prepared by four different methods including alcohol-heating (AH), sol–gel (SG), co-precipitation (CP) and solid reaction (SR) methods. All the samples appeared the XRD peaks at 2θ = 19.0, 31.3, 36.8, 44.7, 55.8, 59.4, 65.2 and 77.2°, due to (111), (220), (311), (400), (511), and (440) facet diffraction of spinel $MgAl_2O_4$. The $MgAl_2O_4$-SR sample shows the highest crystallinity, while the $MgAl_2O_4$-AH sample shows the relatively low crystallinity with trace amount of MgO. The preparation method indeed exerts a significant effect on the phase structure of $MgAl_2O_4$. After introduction of Pt species, the XRD patterns of all the Pt/$MgAl_2O_4$ catalysts are similar to that of the corresponding $MgAl_2O_4$ support (Fig. 4). The result suggests that the loading of Pt species onto the support makes little change to the structure of the support. It is worth noting that no XRD peaks of Pt particles were detected on all the catalysts, suggesting that Pt species were highly dispersed on the surface of these catalysts.

Figure 5 showed the SEM images of Pt/$MgAl_2O_4$ catalyst prepared by four methods. It can be seen that the synthesis method had a significant impact on the morphology of the catalysts. Pt/$MgAl_2O_4$-AH shows the flower-like morphology composed of polymerized lamellae, the

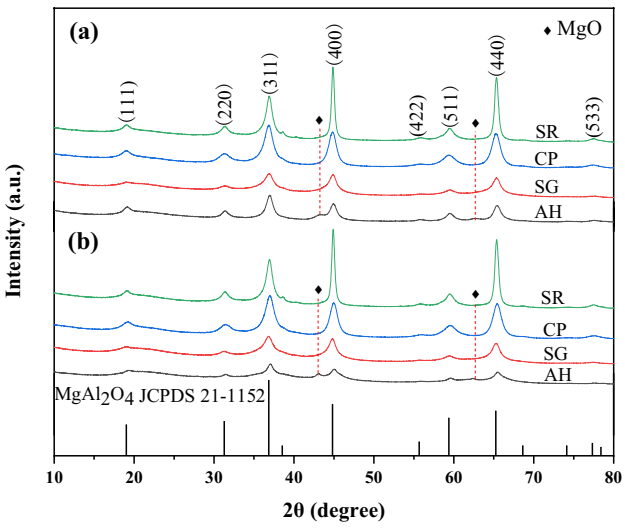


**Fig. 4** XRD patterns of the $MgAl_2O_4$ support and Pt/$MgAl_2O_4$ prepared by different methods: a $MgAl_2O_4$ and b Pt/$MgAl_2O_4$

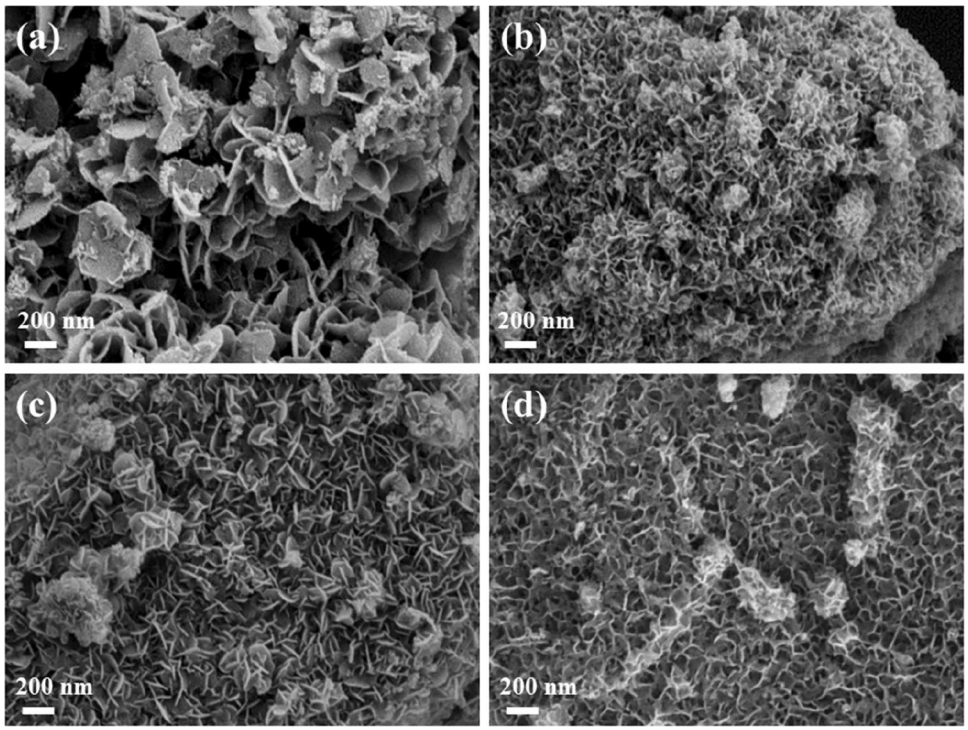


**Fig. 5** SEM images of Pt/$MgAl_2O_4$ prepared by different methods: **a** Pt/$MgAl_2O_4$-AH, **b** Pt/$MgAl_2O_4$-SG, **c** Pt/$MgAl_2O_4$-CP, **d** Pt/$MgAl_2O_4$-SR

sheet structure is also the main morphology features for the Pt/$MgAl_2O_4$-CP catalysts, but size is as small as about 100 nm. Pt/$MgAl_2O_4$-SG and Pt/$MgAl_2O_4$-SR displays an irregular network structure. It may be due that the uniform sheet interlinked with each other to form a structure like a nest. In comparison, Pt/$MgAl_2O_4$-SG was formed by smaller nest than the Pt/$MgAl_2O_4$-SR sample.

The TEM images of the catalysts after $H_2$ reduction treatment are shown in Fig. 6. It can be seen that Fig. 6b–d indicate some obvious dark dots, indicating that Pt species is not uniformly dispersed and relatively large particles are formed due to the agglomeration and sintering. Comparatively, there are no visible dark dots of Pt nanoparticles in Fig. 6a, suggesting that the Pt/$MgAl_2O_4$-AH possesses relatively uniform Pt active sites. Besides, it can be seen from the particle size distribution diagram the particle size of Pt species on Pt/$MgAl_2O_4$-AH and Pt/$MgAl_2O_4$-SG is narrow and concentrated in 0.5–2.5 and 0.5–3.5 nm, respectively. The particle size distribution of Pt/$MgAl_2O_4$-AH was narrower than Pt/$MgAl_2O_4$-SG obviously. The Pt/$MgAl_2O_4$-CP and Pt/$MgAl_2O_4$-SR showed large particle size of Pt in the range of 1–6 nm. The TEM images of representative catalysts before and after reaction were shown in Fig. S4. It can be seen that the Pt particles of the catalysts after reaction have increased to a certain extent. It showed agglomeration of Pt particles during the dehydrogenation of decalin. But the Pt/$MgAl_2O_4$-AH catalyst after reaction still maintain relatively narrow particle size distribution.

The specific surface area and pore characteristics of Pt/$MgAl_2O_4$ prepared by four different methods were characterized by nitrogen adsorption desorption as shown in Figs. S5 and S6. The pore size distribution was obtained by BJH method of $N_2$ adsorption isotherm. According to IUPAC classification, all catalysts exhibited a type IV isotherm with H3 hysteresis loops, with obvious mesoporous distribution [35]. The physicochemical characteristics of the four Pt/$MgAl_2O_4$ catalysts were presented in Table 2. Both the specific surface area ($S_{BET}$) and total pore volume ($V_p$) of these catalysts decrease in the order of Pt/$MgAl_2O_4$-AH > Pt/$MgAl_2O_4$-SG > Pt/$MgAl_2O_4$-CP > Pt/$MgAl_2O_4$-SR. Among the four synthesized catalysts, Pt/$MgAl_2O_4$-AH shows the largest specific surface area and pore volume, which should be more favorable for the decalin dehydrogenation reaction. Comparison from the data in Tables 2 and S2 indicate that addition of Pt does not significantly change the textural properties of the supports. In addition, the final Pt loadings were accurately determined by ICP-AES to be 0.921, 0.866, 0.994 and 0.806 wt% for the four catalysts as shown in Table 2. The results of CO chemisorption in Table 2 showed that the Pt dispersion in the catalysts was increased from 37.2 to 76.3% and thus the size of Pt nanoparticle decreased from 3.74 to 1.24 nm. Especially, Pt/$MgAl_2O_4$-AH had the highest metal dispersion and the smallest mean size of Pt particles.

It was reported that the dehydrogenation performance of n-Butane was closely related to the surface acidity of catalysts [36]. The strong acidity can strengthen the metal-support interaction and leads to improved metal dispersion

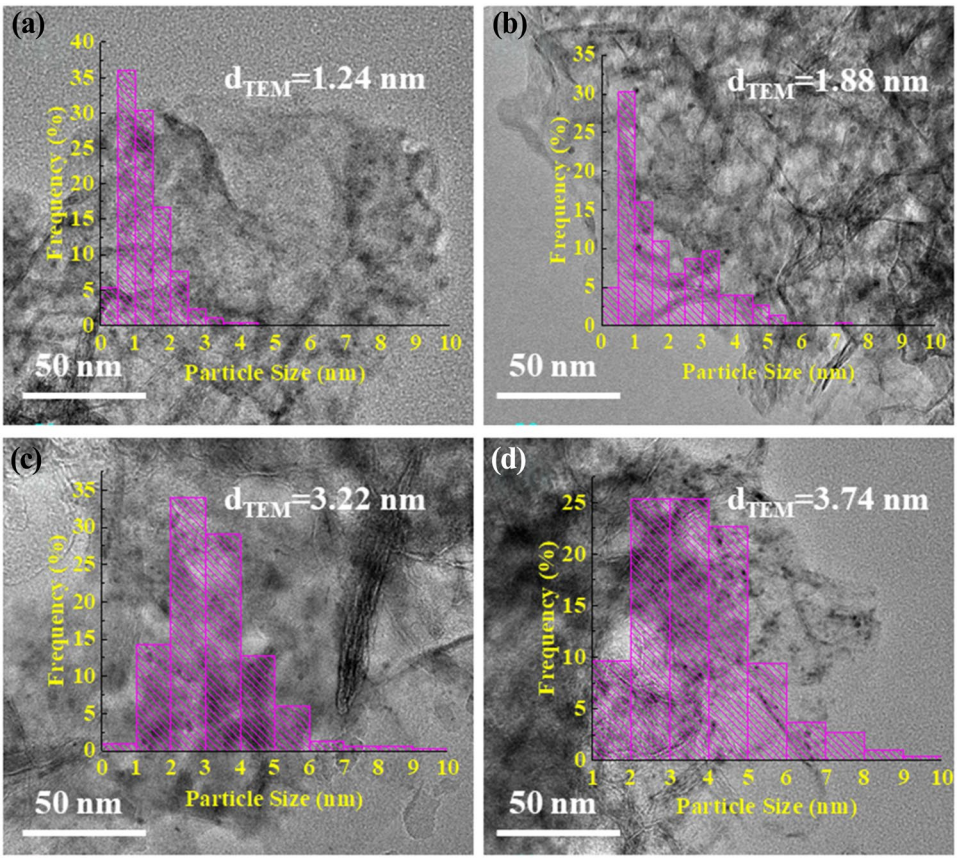


**Fig. 6** TEM images of Pt/$MgAl_2O_4$ prepared by different methods: **a** Pt/$MgAl_2O_4$-AH; **b** Pt/$MgAl_2O_4$-SG; **c** Pt/$MgAl_2O_4$-CP; **d** Pt/$MgAl_2O_4$-SR

and decreased metal particle size, which is conducive to the dehydrogenation reaction. In order to compare the effect of preparation method on the surface acidity of catalysts, the $NH_3$-TPD characterization was performed and the results are shown in Fig. 7. The method of combining the Gaussian curve fitting was used to solve the convolution of the $NH_3$-TPD curve to obtain a semi-quantitative analysis of acid intensity distribution and total acidity. The fitted peaks are shown in Fig. S7, and the multi-peak fitting results were listed in Table 2. According to the definition of acidity, ammonia analysis in the temperature range of 100–130 and 170–210 °C are regarded as weak acid sites, and the peaks at 340–450 and 530–620 °C were regarded as medium and strong acid sites, respectively. These results shows that the synthesis method could affect the acidity of the catalyst, and the amounts of total and strong acid sites of Pt/$MgAl_2O_4$-AH were significantly higher than the other catalysts, which can be contributed to strengthening the metal-support interaction and achieving small Pt nanoparticle size.

Figure 8 is the variation curve of hydrogen production with reaction time when 1 mL decalin was added to the surface of 0.3 g Pt/$MgAl_2O_4$ catalyst at 260 °C. The hydrogen production curve with reaction time can be obviously divided into two stages: the initial 30 min, i.e. the initial rapidly increasing hydrogen production stage and the later stage of the reaction from 30 to 150 min for a levelled off the of dehydrogenation rate.

The reason why the whole reaction process was obviously divided into two periods is mainly caused by different reaction mechanisms. In the early induction period, the reflux rate of droplet was very fast and the droplet contained more unreacted decalin relative to the product for fast reaction rate. It is also possible that the surface of the catalyst was still undergoing a conditioning stage before a stabilized surface composition were formed after a short period of reaction. At a high temperature, dehydrogenation reaction occurred on the catalyst surface to generate liquid products and release hydrogen. At the same time, the products and unreacted decalin quickly absorbed heat and vaporized away from the catalyst surface, then condensed through the condensation pipe and dripped back to the catalyst surface. Therefore, the reaction at this stage is a gas–liquid–solid heterogeneous reaction, which can form a liquid film on the surface of the catalyst and then achieved the fast hydrogen productivity. The heat provided by the high-temperature catalyst was used to not only promote the dehydrogenation reaction, but also vaporize the liquid after the reaction away from the solid surface.

At the same time, the products and unreacted decalin quickly absorbed heat and vaporized away from the catalyst

**Table 2** Physicochemical characteristics of Pt/$MgAl_2O_4$ prepared by different methods and the semi-quantitative results of $NH_3$-TPD measurements

| Catalysts | $S_{BET}$[a] ($m^2\ g^{-1}$) | $V_p$[b] ($cm^3\ g^{-1}$) | $D_m$[c] (nm) | Pt[d] (wt%) | particle size (nm)[e] | Pt dispersion(%)[f] | Total area (a.u.) | Peak area fraction (%) | | |
|---|---|---|---|---|---|---|---|---|---|---|
| | | | | | | | | weak acid sites | medium acid sites | strong acid sites |
| Pt/$MgAl_2O_4$-AH | 307 | 0.92 | 11.3 | 0.921 | 1.24 | 76.3 | 48,684 | 43.4 | 29.6 | 27.0 |
| Pt/$MgAl_2O_4$-SG | 184 | 0.49 | 10.7 | 0.866 | 1.88 | 65.2 | 34,653 | 60.2 | 13.8 | 26.0 |
| Pt/$MgAl_2O_4$-CP | 110 | 0.30 | 11.1 | 0.994 | 3.22 | 52.1 | 30,536 | 55.3 | 19.4 | 25.3 |
| Pt/$MgAl_2O_4$-SR | 75 | 0.13 | 6.9 | 0.806 | 3.74 | 37.2 | 18,583 | 46.3 | 38.7 | 15.0 |

[a]$S_{BET}$ is the specific surface area calculated by BET method
[b]$V_p$ is the total pore volume
[c]$D_m$ is the mean pore size
[d]Pt is the content determined by ICP-AES
[e]Average Pt particle size obtained by fitting TEM data
[f]Based on CO chemisorption

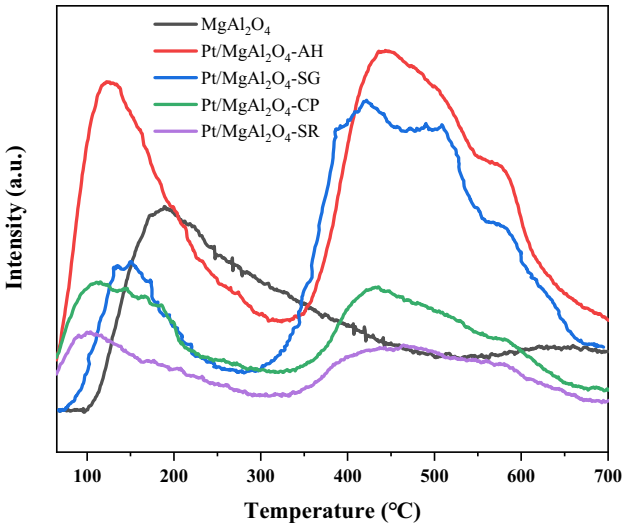


**Fig. 7** $NH_3$-TPD profiles for Pt/$MgAl_2O_4$ prepared by different methods

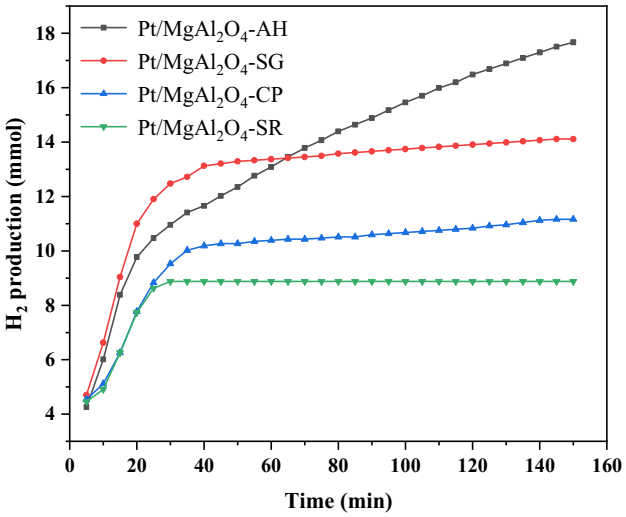


**Fig. 8** Hydrogen production yield over Pt/$MgAl_2O_4$ catalysts prepared by different methods

surface, then condensed through the condensation pipe and dripped back to the catalyst surface. Therefore, the reaction at this stage is a gas–liquid–solid heterogeneous reaction, which can form a liquid film on the surface of the catalyst and then achieved the fast hydrogen productivity. The heat provided by the high-temperature catalyst was used to not only promote the dehydrogenation reaction, but also vaporize the liquid after the reaction away from the solid surface. It can be observed from Fig. 8 that the hydrogen production rates over the four catalysts are in the order of Pt/$MgAl_2O_4$-AH > Pt/$MgAl_2O_4$-SG > Pt/$MgAl_2O_4$-CP > Pt/$MgAl_2O_4$-SR at the same reaction time. The characterization result had shown that $MgAl_2O_4$ prepared by different

synthesis methods generated different physical and chemical properties. Firstly, the particle size of active component had an important influence on the reaction activity. Highly dispersed small particle size are conducive to the reaction rate. Obviously, the final $H_2$ production was consistent with the particle size of Pt particle. The Pt/$MgAl_2O_4$-AH catalyst showed good dispersion of Pt species and the mean particle size was less than 1 nm. The synthesis methods also yielded an effect on the crystallinity of support and the size of Pt particle, which in turn influence the catalytic performance. The Pt/$MgAl_2O_4$-AH possesses the largest BET surface area and pore volume, as well as the highest $H_2$ production in the four catalysts. The large specific surface area and pore volume are conducive to diffusion and accessibility of the active sites to the reactant and intermediate. Therefore, the physical properties such as the specific surface area and pore volume should play an important part in reaction activity. It had been found that the catalyst in liquid film state can ensure high reaction temperature and large surface contact area, and realize the maximum hydrogen evolution of decalin [8, 18, 37], which should be closely related to the physical properties of catalysts. During the reaction, the contact state between the catalyst and reactants was distinctly different when 1 mL of decalin was added. The Pt/$MgAl_2O_4$-AH possessed the largest BET surface area and pore volume, and this forms a so-called liquid-film state. However, the Pt/$MgAl_2O_4$-CP catalyst with small BET surface area and pore volume was dispersed in the reactant in a suspended state when 1 ml of decalin was added, which is not favorable to the reaction.

These results show that alcohol-heating method is the best method to synthesis the $MgAl_2O_4$ supported Pt-based catalysts. In addition, the composition of support usually can also influence the properties and performance of catalysts. Herein, the effect of Mg/Al molar ratio of $MgAl_2O_4$ was further studied.

### 3.3 Effect of Mg/Al Molar Ratio of $MgAl_2O_4$

Figure 9 shows the XRD patterns of the $MgAl_2O_4$ and Pt/$MgAl_2O_4$ with different Mg/Al molar ratios. The characteristic peaks of spinel $MgAl_2O_4$ (JCPDS No. 21-1152) were found only for the sample synthesized with Mg/Al molar ratio of 0.5. When the Mg/Al molar ratio was not the theoretical value of 0.5, no significant diffractions corresponding to the spinel $MgAl_2O_4$ were detected. Instead, the catalysts with Mg/Al molar ratio > 0.5 presented periclase MgO as the primary crystal phase. With increasing Mg/Al molar ratio, the intensity of diffraction peaks assigned to MgO increased, indicating that more MgO crystalline phases were formed. However, the Mg or Al oxides existed mainly as amorphous phase for the catalysts with Mg/Al molar ratio < 0.5. Moreover, the diffraction peaks of Pt species were not detected for all the catalysts because of their small particle size.

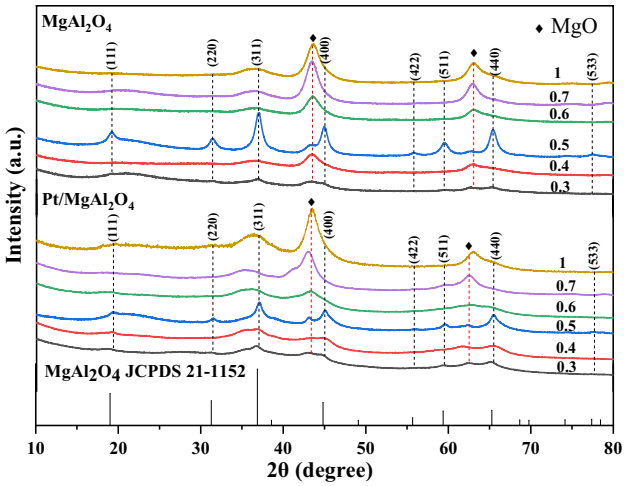


**Fig. 9** XRD patterns of $MgAl_2O_4$ and Pt/$MgAl_2O_4$ with different Mg/Al molar ratio

**Table 3** Textural properties of Pt/$MgAl_2O_4$ with different Mg/Al molar ratio

| Mg/Al(molar ratio) | $S_{BET}$[a] ($m^2\ g^{-1}$) | $V_p$[b] ($cm^3\ g^{-1}$) | $D_m$[c] (nm) |
|---|---|---|---|
| 0.3 | 393 | 0.77 | 7.82 |
| 0.4 | 324 | 0.47 | 5.75 |
| 0.5 | 307 | 0.92 | 11.33 |
| 0.6 | 323 | 0.62 | 7.69 |
| 0.7 | 268 | 1.05 | 16.02 |
| 1 | 365 | 0.46 | 4.99 |

[a]$S_{BET}$ the specific surface area calculated by BET method

[b]$V_p$ the total pore volume

[c]$D_m$ the mean pore size

Nitrogen adsorption–desorption experiments (Fig. S8) were carried out to investigate the specific surface area and pore characteristics of all samples. Type IV adsorption–desorption isotherms with H3 hysteresis loop were observed for all the samples, suggesting that samples were typical ordered mesoporous materials. Figure S9 shows that the pore size distributions of catalysts with different Mg/Al molar ratios determined by the BJH model according to the desorption branches of the isotherms. As shown in Fig. S9, the Mg/Al molar ratio produces an influential effect on the pore size distribution of the catalysts. The pore size varies with the Mg/Al molar ratio. In general, the synthesized catalysts maintain a mesoporous structure with pore sizes mainly distributed in the range of 1–10 nm.

The specific surface area and pore structure parameters of the support can affect the state of active components and the internal diffusion process to some extent, and then affect the catalytic performance of catalysts. Table 3 shows the BET

specific surface area, pore volume and mean pore diameter of catalysts with different Mg/Al molar ratios. Both specific surface area and pore volume are relatively high for the sample with Mg/Al molar ratio of 0.5. The activity of decalin dehydrogenation should be closely related to the textural properties. It should be the moderate balance of specific surface area, pore volume and uniform pore-size distribution.

The SEM micrographs of samples with different Mg/Al molar ratios were shown in Fig. 10. Obviously, Mg/Al ratio had a significant effect on the morphology. All the samples still show the flower-like morphology composed of interlinked nanosheets, but the size of $MgAl_2O_4$ nanosheets increases with growing Mg/Al molar ratio. When Mg/Al molar ratio increases from 0.6 to 1, more complex pore structures can be observed on the samples. These results are consistent with the $N_2$ adsorption–desorption results. Figure 11 shows the TEM morphology and the corresponding Pt nanoparticle size distribution histogram of the representative samples. It is obvious that the sample with Mg/Al molar ratio of 0.5 generates the smallest average particle size of 1.24 nm. In general, too low or too high proportion of Mg can yield a negative effect on the Pt nanoparticle distribution. The results show that the proportion of Mg can significantly modify the size distribution of Pt particles.

Figure 12a showed the $H_2$ production rate from decalin dehydrogenation over the Pt/$MgAl_2O_4$ catalysts with different Mg/Al molar ratios. When Mg/Al molar ratio increases from 0.3 to 1.0, the $H_2$ production of the samples increases gradually and reaches the maximum value of 17.7 mmol at the Mg/Al molar ratio of 0.5, and then decreases gradually. The $H_2$ production of Pt/$MgAl_2O_4$ with Mg/Al molar ratio of 0.5 is almost twice that of the sample with Mg/Al molar ratio of 0.3. Figure 12b shows the "apparent" TOF value of hydrogen production with different Mg/Al molar ratio. It can be seen that the catalyst with Mg/Al molar ratio of 0.5 generates the highest TOF of hydrogen production, while other catalysts produce roughly the same TOF, indicating that the active sites are different. The high dehydrogenation efficiency of catalyst with Mg/Al molar ratio of 0.5 should be attributed to the relatively small Pt particles. These results indicated that too small or too large Mg/Al molar ratio was unfavorable to the dehydrogenation of decalin. The stoichiometric molar ratio of Mg/Al seemed to be suitable for the $MgAl_2O_4$ formation in the Pt/$MgAl_2O_4$ catalyst. However, the mechanism of Mg/Al molar ratio effect on the decalin dehydrogenation is complex. On one hand, the Mg/Al molar ratio of $MgAl_2O_4$ support generated effects on the physicochemical properties of Pt/$MgAl_2O_4$ catalyst including crystallinity, morphology, surface acidity and textual properties, which usually can in turn influence the Pt nanoparticle size distribution. It is well known that the Pt nanoparticle size is one of the most critical factors in determining the catalytic performance of decalin dehydrogenation. The small size of Pt nanoparticle is conducive to the reaction activity. The TEM results indeed demonstrate that the Pt/$MgAl_2O_4$ with Mg/Al molar ratio of 0.5 shows the smallest average particle size of 1.24 nm. On the other hand, the Mg/Al molar ratio of $MgAl_2O_4$ support shows the effect on the textual properties of catalyst and then had the direct effect on the contacting state of reaction system. Since the contacting state between catalyst and reactant also exerts a great influence on the dehydrogenation reaction rate of decalin. It was found that there were an optimal ratio between catalyst and reactant to make it in the "liquid-film" state and achieved the best catalytic activity at this time. The state of liquid-film may be related to specific surface area and pore volume as well

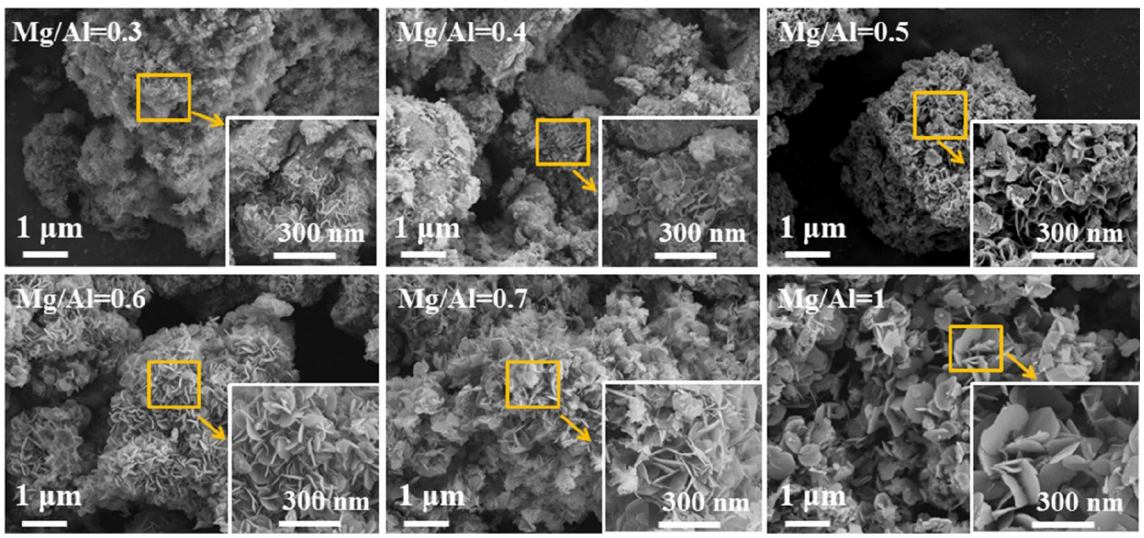


**Fig. 10** SEM images of Pt/$MgAl_2O_4$ with different Mg/Al molar ratio

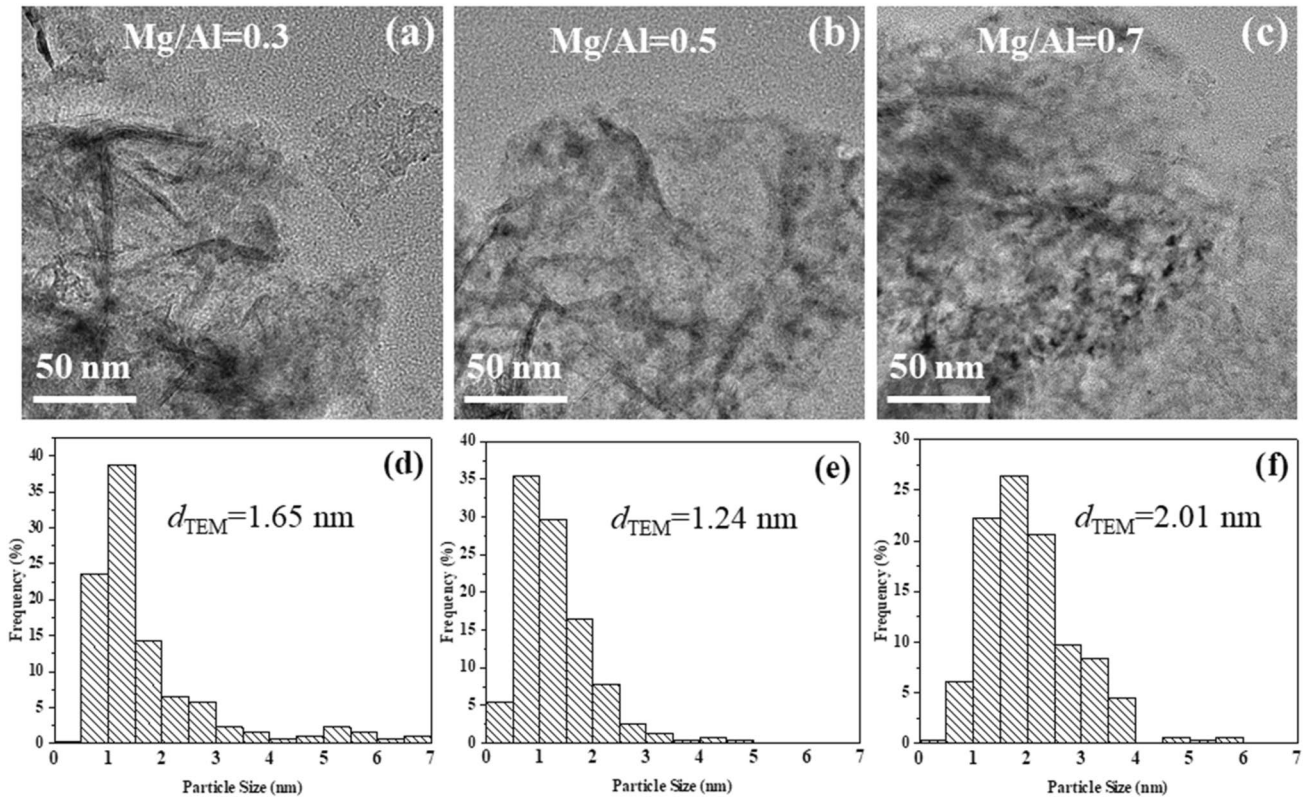


**Fig. 11** TEM images (**a**–**c**) and corresponding particle size distribution (**d**–**f**) of $Pt/MgAl_2O_4$ with different Mg/Al molar ratio

as pore-size distribution. Therefore, the relevant contents about the "liquid-film" states were further investigated and discussed in the next part.

### 3.4 Effect of Reactant Feeding Rate of Decalin

The hydrogen evolution from decalin dehydrogenation was further performed in various amounts of decalin (0.5, 0.75, 1.0, 1.25 and 1.5 mL) reactant loadings over a constant amount (0.3 g) of $Pt/MgAl_2O_4$ catalyst under boiling (260 °C heating) and refluxing (5 °C cooling) conditions. Figure 13 shows the effect of initial amount of decalin on the catalytic dehydrogenation of $Pt/MgAl_2O_4$. The $H_2$ production were strongly dependent on the initial feeding amount of decalin. Hodoshima [32] and Kariya [33] et al. also found that the dehydrogenation rate of decalin was closely related to the initial ratio of decalin to catalyst and usually reached the maximum in the liquid-film state.

Via changing the ratio of liquid reactant volume to solid catalyst at a certain reaction temperature, the dehydrogenation reaction system can appear in three different reaction states, i.e., suspended state, liquid-film state and sand-bath state [8]. The liquid-film state refers to the appropriate proportion of liquid reactant volume and catalyst mass, and the evaporation and condensation rates of liquid are equivalent. The dehydrogenation reaction generally occurs at high temperature, while the organic liquid vaporizes away from the catalyst surface, and then drops back to the catalyst surface through condensation. The catalyst system in the liquid-film state is alternately wetted by the condensed liquid, proceeds to the catalytic reaction, and then evaporates to form dry surface. Therefore, this reaction mode was also called "wet-dry multiphase" dehydrogenation reaction mode [33].

If the initial amount of reactant is too large, the excess liquid reactant always covers the catalyst surface, and the reaction conditions are equivalent to the liquid phase reaction. As shown in Fig. 13, the hydrogen evolution rates for the decalin amount of 1.5 mL were relatively low from the beginning, and then resulted in a low hydrogen production. Besides, in the cases of too small decalin amount, the surface of catalyst was not completely wetted and easy to become dry in less than 20 min after the reaction. As dehydrogenation reaction still proceeded, the amount of liquid decreased with the evaporation of naphthalene. Since naphthalene is more volatile than decalin and the empty space in the reactor is sufficiently large, the supply of decalin was easy to decrease over time. As a result, the initial dehydrogenation reaction rate decreased rapidly, and the conversion basically remained unchanged in 2.5 h or later, as if the catalyst was in a wet sand-bath state.

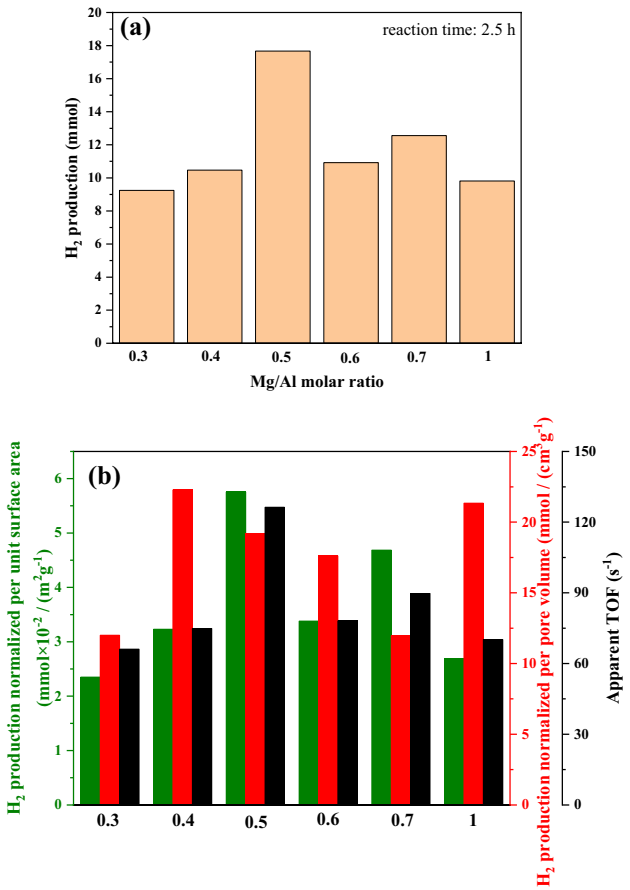


**Fig. 12** **a** $H_2$ production and **b** $H_2$ production normalized per unit surface area, pore volume and "apparent" TOF as a function of Mg/Al molar ratio over Pt/$MgAl_2O_4$. Reaction condition: 2.5 h, 260 °C, 0.3 g of catalyst and 1 mL of decalin

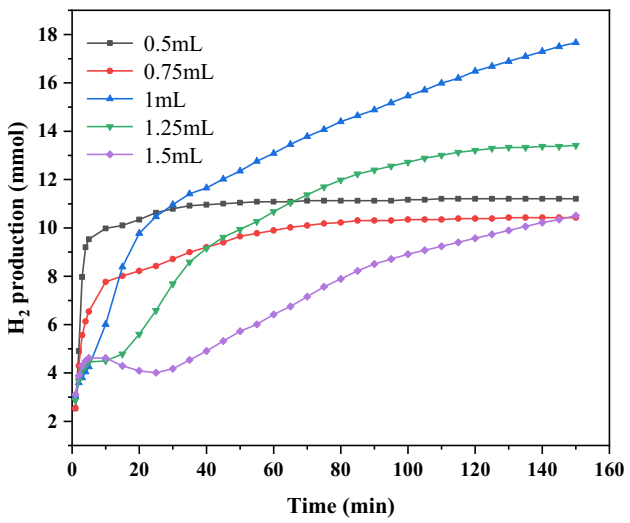


**Fig. 13** Time-dependent $H_2$ production with 0.3 g Pt/$MgAl_2O_4$ catalyst at various charged amounts of decalin in batch-wise operation

The appropriate amount of liquid reactant made the catalyst surface covered with a layer of overheated decalin liquid film. This is generally considered to be the superheated liquid-film state under reactive distillation conditions [33, 38]. At this time, the surface temperature of the catalyst was higher than the boiling point of the reactant decalin. At the same time, the continuous boiling reflux of superheated decalin ensured that the catalyst was wet enough. The above analysis showed that the catalyst system in liquid-film state can ensure higher reaction temperature and larger contact area, and then showed excellent catalytic performance. The amount of liquid reactant in the liquid-film state was related to specific surface area and pore volume as well as pore-size distribution of the catalyst. Indeed, the support style, preparation method and Mg/Al molar ratio show the significant effect on the chemical structure and environment of catalysts, especially the size of Pt nanoparticle. However, it was worth noting that the textural properties such as specific surface area, pore volume and pore-size distribution also changed distinctly for the supports with different style, preparation method or Mg/Al molar ratio, which tended to influence the condition of liquid film state. Figure 12b showed the $H_2$ production normalized per unit surface area and pore volume as a function of Mg/Al molar ratio over Pt/$MgAl_2O_4$. Obviously, the normalized $H_2$ production was not influenced only by any factor. Actually, the direct influence of the textural properties on the $H_2$ production should be the moderate balance of specific surface area and pore volume basically. This effect was essentially evenly split between specific surface area and pore volume as the dotted line shown in Fig. 12b. Therefore, the dehydrogenation process of decalin is determined by multiple factors.

## 4 Conclusion

In this work, four common supports including $Al_2O_3$, MCM-41, AC and $MgAl_2O_4$ were selected to prepare the supported Pt-based catalysts to study the influences of the preparation method and Mg/Al molar ratio of $MgAl_2O_4$ on material properties and the catalytic performance. The results show that the Pt/$MgAl_2O_4$ catalyst with the $MgAl_2O_4$ support synthesized via alcohol-heating method with stoichiometric ratio of Mg/Al yields the best catalytic performance. $MgAl_2O_4$ support is more beneficial to the interaction between Pt species and support and can achieve smaller Pt nanoparticle size of about 1.24 nm. The preparation method and Mg/Al molar ratio of $MgAl_2O_4$ support also play an important role in the physicochemical properties of Pt/$MgAl_2O_4$ catalyst, including crystallinity, morphology, surface acidity, textual properties and notably Pt nanoparticle size distribution. These influencing factors can have direct or indirect effect on the catalytic performance. Particularly,

the size of Pt nanoparticle cab be modified by different support types, preparation methods and Mg/Al molar ratios to achieve properly small particle size that is more favorable to decalin dehydrogenation. Furthermore, it was found that the $H_2$ production was also strongly dependent on the initial ratio of decalin to catalyst. The optimal ratio was achieved in a transitional reaction state between gas and liquid phase reaction, i.e. the liquid-film state, which should be the moderate balance of specific surface area and pore volume. This study will help to design and modify the efficient decalin dehydrogenation catalyst, and is of great significance to the application of liquid-phase organic hydride hydrogen storage technology.

**Supplementary Information** The online version contains supplementary material available at https://doi.org/10.1007/s10562-023-04283-5.

**Acknowledgements** This work was supported from the National Natural Science Foundation of China (22202013), Beijing Education Committee Science and Technology Project (KM202110017010) and the special fund from the Beijing Institute of Petrochemical Technology (Grant No. 15031862004-1).

**Funding** Special Fund from Beijing Institute of Petrochemical Technology (15031862004-1) and the Beijing Education Committee Science and Technology Project (KM202110017010).

## Declarations

**Competing interest** The authors declare that they have no known competing financial interests or personal relationships that could have appeared to influence the work reported in this paper.

## References

1. Liu Z, Guan D, Wei W, Davis SJ, Ciais P, Bai J, Peng S, Zhang Q, Hubacek K, Marland G (2015) Reduced carbon emission estimates from fossil fuel combustion and cement production in China. Nature 524:335–338
2. Zheng J, Zhou H, Wang CG, Ye E, Xu JW, Xian JL, Li Z (2021) Current research progress and perspectives on liquid hydrogen rich molecules in sustainable hydrogen storage-ScienceDirect. Energy Storage Mater 35:695–722
3. Shukla A, Karmakar S, Biniwale RB (2012) Hydrogen delivery through liquid organic hydrides: considerations for a potential technology. Int J Hydrog Energy 37:3719–3726
4. Biniwale RB, Rayalu S, Devotta S, Ichikawa M (2008) Chemical hydrides: a solution to high capacity hydrogen storage and supply. Int J Hydrog Energy 33:360–365
5. Ninomiya W, Tanabe Y, Sotowa KI, Yasukawa T, Sugiyama S (2008) Dehydrogenation of cycloalkanes over noble metal catalysts supported on active carbon. Res Chem Intermed 34:663–668
6. Ninomiya W, Tanabe Y, Uehara Y, Sotowa KI, Sugiyama S (2006) Dehydrogenation of tetralin on Pd/C and Te-Pd/C catalysts in the liquid-film state under distillation conditions. Catal Lett 110:191–194
7. Pande JV, Shukla A, Biniwale RB (2012) Catalytic dehydrogenation of cyclohexane over Ag-M/ACC catalysts for hydrogen supply. Int J Hydrog Energy 37:6756–6763
8. Saito Y, Aramaki K, Hodoshima S, Saito M, Shono A, Kuwano J, Otake K (2008) Efficient hydrogen generation from organic chemical hydrides by using catalytic reactor on the basis of superheated liquid-film concept-ScienceDirect. Chem Eng Sci 63:4935–4941
9. Tien PD, Satoh T, Miura M, Nomura M (2008) Continuous hydrogen evolution from cyclohexanes over platinum catalysts supported on activated carbon fibers. Fuel Process Technol 89:415–418
10. Wang Y, Shah N, Huffman GP (2004) Pure hydrogen production by partial dehydrogenation of cyclohexane and methylcyclohexane over nanotube-supported Pt and Pd catalysts. Energy Fuels 18:1429–1433
11. Zhao J, Qi P, Xu J, Tao F (2014) Current situation and prospect of hydrogen storage technology with new organic liquid. Int J Hydrog Energy 39:17442–17451
12. Luo M, Christine CW (1996) Thermal and catalytic coprocessing of Illinois No 6. coal with model and commingled waste plastics. Fuel Process Technol 49:91–117
13. Chen A, Zhang W, Li X, Tan D, Han X, Bao X (2007) One-pot encapsulation of Pt nanoparticles into the Mesochannels of SBA-15 and their catalytic dehydrogenation of methylcyclohexane. Catal Lett 119(1):159–164
14. Du J, Zhao R, Jiao G (2013) The short-channel function of hollow carbon nanoparticles as support in the dehydrogenation of cyclohexane. Int J Hydrog Energy 38:5789–5795
15. Shinohara C, Kawakami S, Moriga T, Hayashi H, Hodoshima S, Saito Y, Sugiyama S (2004) Local structure around platinum in Pt/C catalysts employed for liquid-phase dehydrogenation of decalin in the liquid-film state under reactive distillation conditions. Appl Catal A 266:251–255
16. Shukla AA, Gosavi PV, Pande JV, Kumar VP, Chary K, Biniwale RB (2010) Efficient hydrogen supply through catalytic dehydrogenation of methylcyclohexane over Pt/metal oxide catalysts. Int J Hydrog Energy 35:4020–4026
17. Martynenko EA, Pimerzin AA, Savinov AA, Verevkin SP, Pimerzin AA (2020) Hydrogen release from decalin by catalytic dehydrogenation over supported platinum catalysts. Top Catal 63:178–186
18. Sebastian D, Bordeje EG, Calvillo I, Lazaro MJ, Moliner R (2008) Hydrogen storage by decalin dehydrogenation/naphthalene hydrogenation pair over platinum catalysts supported on activated carbon. Int J Hydrog Energy 33:1329–1334
19. Ping L, Huang YL, Chen D, Zhu J, Zhao TJ, Zhou XG (2009) CNFs-supported Pt catalyst for hydrogen evolution from decalin. Catal Commun 10:815–818
20. A Y T, A H J, A X L et al (2016) Kinetic behavior of Pt catalyst supported on structured carbon nanofiber bed during hydrogen releasing from decalin[J]. Int J Hydrog Energy 41(25):10755–10765
21. Tuo YX, Shi LJ, Cheng HY et al (2018) Insight into the support effect on the particle size effect of Pt/C catalysts in dehydrogenation[J]. J Catal 360:175–186
22. Rahmat N, Yaakob Z, Hassan N (2021) Hydrogen rich syngas from $CO_2$ reforming of methane with steam catalysed by facile fusion-impregnation of iron and cobalt loaded $MgAl_2O_4$ catalyst with minimal carbon deposits. J Energy Inst 96:61–74
23. Jiao Y, Chen T, Wang L, Yao P, Zhang J, Chen Y, Chen Y, Wang J (2020) Synthesis of a high-stability nanosized Pt-loaded $MgAl_2O_4$ catalyst for n-decane cracking with enhanced activity and durability. Ind Eng Chem Res 59:4338–4347
24. Yu S, Hu Y, Cui H, Cheng Z, Zhou Z (2021) Ni-based catalysts supported on $MgAl_2O_4$ with different properties for combined steam and $CO_2$ reforming of methane. Chem Eng Sci 232:116379
25. Yang J, Peng M, Ren G, Qi H, Zhou X, Xu J, Deng F, Chen Z, Zhang J, Liu K (2020) A hydrothermally stable irreducible

oxide-Modified Pd/$MgAl_2O_4$ catalyst for methane combustion. Angew Chem 132:18680–18684
26. Khoja AH, Tahir M, Amin NAS, Javed A, Mehran MT (2020) Kinetic study of dry reforming of methane using hybrid DBD plasma reactor over $La_2O_3$ co-supported Ni/$MgAl_2O_4$ catalyst. Int J Hydrog Energy 45:12256–12271
27. Bocanegra S, YañezScelzade Miguel MJOS (2010) Effect of the synthesis method of $MgAl_2O_4$ and of Sn and Pb addition to platinum catalysts on the behavior in n-butane dehydrogenation. Ind Eng Chem Res 49:4044–4054
28. Zhang X, Qi M, Zhang GQ, Lin T, Gong T (2011) Solvent-Free liquid phase oxidation of benzyl alcohol to benzaldehyde over superfine $MgAl_2O_4$ supported Co-based catalysts: effects of support $MgAl_2O_4$. Adv Mater Res 233–235:1100–1107
29. Bocanegra SA, Ballarini AD, Scelza OA, Miguel S (2008) The influence of the synthesis routes of $MgAl_2O_4$ on its properties and behavior as support of dehydrogenation catalysts. Mater Chem Phys 111:534–541
30. Wang F, Li WZ, Lin JD, Chen ZQ, Wang Y (2018) Crucial support effect on the durability of Pt/$MgAl_2O_4$ for partial oxidation of methane to syngas. Appl Catal B 231:292–298
31. Tuo Y, Meng Y, Chen C, Lin D, Zhang J (2021) Partial positively charged Pt in Pt/$MgAl_2O_4$ for enhanced dehydrogenation activity. Appl Catal B 288:119996
32. Hodoshima S, Arai H, Saito Y (2003) Liquid-film-type catalytic decalin dehydrogeno-aromatization for long-term storage and long-distance transportation of hydrogen. Int J Hydrog Energy 28:197–204
33. Kariya N, Fukuoka A, Ichikawa M (2002) Efficient evolution of hydrogen from liquid cycloalkanes over Pt-containing catalysts supported on active carbons under "wet-dry multiphase conditions." Appl Catal A 233:91–102
34. Feng Z, Chen X, Bai X (2020) Catalytic dehydrogenation of liquid organic hydrogen carrier dodecahydro-N-ethylcarbazole over palladium catalysts supported on different supports. Environ Sci Pollut Res 27:36172–36185
35. Thommes M (2016) Physisorption of gases, with special reference to the evaluation of surface area and pore size distribution (IUPAC Technical Report). Pure Appl Chem 87:25–25
36. Bocanegra S, Yanez MJ, Scelza O, Miguel SD (2010) Effect of the synthesis method of $MgAl_2O_4$ and of Sn and Pb addition to platinum catalysts on the behavior in n-Butane dehydrogenation. Ind Eng Chem Res 49:4044–4054
37. Sugiyama S, Shinohara C, Makino D, Kawakami S, Hayashi H (2006) Liquid film state under reactive distillation conditions for the dehydrogenation of decalin on platinum supported on active carbon and boehmite. New Dev Appl Chem Reaction Eng 159:281–284
38. Kariya N, Fukuoka A, Utagawa T, Sakuramoto M, Ichikawa M (2003) Efficient hydrogen production using cyclohexane and decalin by pulse-spray mode reactor with Pt catalysts. Appl Catal A 247:247–259